Learning-Based Guidance and Control Codesign for Underactuated Autonomous Surface Vehicles: Theory and Experiment

Li-Ying Hao, *Senior Member, IEEE*, Yun-Peng Liu, Zhi-Jie Wu, and Chao Shen, *Member, IEEE*

***Abstract*—Traditional sideslip angle estimator compensation methods used in line-of-sight (LOS) guidance law are not effective when facing with big amplitude and fluctuating sideslip angle scenarios, resulting in poor path following performance of underactuated autonomous surface vehicles (ASVs). To overcome the drawback, a novel sideslip angle estimator based on long short-term memory (LSTM) is proposed in this article. It integrates the selective updated strategy (SUS) to enhance the learning capability and long-term memory of extremely fluctuating temporal information, thereby meeting the requirement of estimating fluctuating sideslip angle. Based on the proposed SUS-LSTM sideslip angle estimator, a learning line-of-sight (LLOS) guidance law for path following is designed. Furthermore, we theoretically prove the input-to-state stability in probability of the closed-loop cascaded control system, which consists of LLOS and heading controller. Finally, the proposed algorithm is implemented on ASVs and experiments are conducted in the Lingshui bay to validate the superiority and effectiveness of the algorithm.**

***Index Terms*—Autonomous surface vehicles (ASVs), long short-term memory (LSTM), path following, selective updated strategy (SUS), sideslip angle estimator.**

I. Introduction

In recent years, the extensive applications of autonomous surface vehicles (ASVs) in reconnaissance, patrol, environmental sampling, marine resource exploration, and coastal surveillance have garnered significant attention [1]. The control system of ASVs exhibits highly coupled states, making motion control a challenging problem. The motion control of ASVs is primarily achieved through the cascade of guidance laws and heading controllers. The guidance laws are employed to generate reference heading angles, ensuring that the ASVs follows the desired path, while the heading controller generates control forces to track the reference heading angles [2].

A popular and effective guidance law for achieving convergence to a desired path is the line-of-sight (LOS) guidance law [3]. In [4], the effectiveness of the traditional LOS method in progressing along a reference path was well demonstrated. During the path following process of underactuated ASVs, an unknown non-zero sideslip angle can be observed due to external disturbances such as wind, waves, and currents, or control forces [5]. The existence of sideslip angles causes non-zero tracking errors, leading to a degraded path following performance.

Researchers have dedicated substantial efforts to enhance the path following performance of ASVs by mitigating the impact of the sideslip angle. In [5], a κ-index stable curved trajectory integral LOS guidance law was further derived, compensating for the constant sideslip angle induced by persistent ocean disturbances. In [6], an adaptive line-of-sight (ALOS) guidance law was introduced, incorporating an adaptive term to identify sideslip angles. A predictor-based LOS approach was proposed [7] to estimate time-varying sideslip angles. Liu et al. [8] introduced low-order extended state observers into classical LOS guidance law design. However, due to the lack of lateral thrust and shallow draft, the sideslip angle of ASVs is usually large and fluctuates sharply during path following. In this case, the estimation of sideslip angle is not good, resulting in poor path following performance [6], [7], [8]. Therefore, it is desired to design a predictor that can accurately estimate the sideslip angle in combination with the path following control, which presents the main motivation of this article.

On the other research front, deep neural networks have made significant advancements and have been widely applied in various fields during the past few years [9]. In [10], a recurrent neural network (RNN) combining input projection layers, regression heads, and gated recurrent units (GRUs) was proposed to estimate sideslip angle. RNN is particularly effective in approximating dynamic systems due to their ability to explicitly capture dependencies over past time steps [11]. Sideslip angle is a variable related to the motion state at the previous time step,

Manuscript received 8 April 2024; revised 16 June 2024; accepted 15 July 2024. This work was supported in part by the National Natural Science Foundation of China under Grant 52171292 and Grant 51939001 and in part by Dalian Outstanding Young Talents Project under Grant 2022RJ05. *(Corresponding author: Li-Ying Hao.)*

Li-Ying Hao, Yun-Peng Liu, and Zhi-Jie Wu are with the Marine Electrical Engineering College, Dalian Maritime University, Dalian 116026, China (e-mail: haoliying@dlmu.edu.cn; lypns0905@163.com; wuzhijie1227@dlmu.edu.cn).

Chao Shen is with the Department of System and Computer Engineering, Carleton University, Ottawa, ON K1S 5B6, Canada (e-mail: shenchao@sce.carleton.ca).

Color versions of one or more figures in this article are available at https://doi.org/10.1109/TIE.2024.3433557.

Digital Object Identifier 10.1109/TIE.2024.3433557

hence employing an RNN to predict sideslip angle is a judicious choice. However, the traditional RNN structure have short-term memory and is prone to losing crucial information from historical data. This attribute limits the ability to learn and retain temporal information with highly fluctuating data [12]. In [13], the long short-term memory-enhanced forget-gate (LSTM-EFG) network was proposed as an improvement over LSTM for wind power data prediction. By adding peepholes and enhancing the means of forgetting gate, the model strengthens the ability of network to learn the historical data fluctuation data. In [14], read-first long short-term memory (RLSTM) increased the read gates to enable interrelations between control gates, thereby enhancing the feature extraction capability during the data encoding phase and strengthening the network's long-term memory. While the models aforementioned in [13], [14] have improved prediction accuracy to some extent, researchers found that their adoption of standard learning strategies, such as gate mechanisms and stochastic optimization, lead to low computational efficiency and the risk of losing vital temporal information acquired from historical observations [15]. Meanwhile, the amplitude of the sideslip angle of ASVs is larger and the variation is more fluctuating than that of the road vehicle. Therefore, we need a neural network with better learning ability, which can extract key information from fluctuating and complex historical data, and then accurately predict the sideslip angle.

In this article, a new selective update strategy long short-term memory (SUS-LSTM) model is designed to meet the demand for prediction of large and fluctuating sideslip angle. Based on the proposed SUS-LSTM sideslip angle estimator, the learning based line-of-sight (LLOS) guidance law is designed to improve the path following effect of ASVs. The main contributions can be summarized as follows:

1) We propose a novel SUS-LSTM model to estimate the sideslip angle due to drift forces induced by ocean disturbances or controlling forces. Different from the traditional standard learning strategies that enhance RNN memory ability [13], [14], the proposed SUS replaces input gate and forget gate to save hidden state information in a more direct way, thus enhancing the learning ability and long-term memory of extreme data variations.
2) With the proposed sideslip angle estimator, we prove the probabilistic input-to-state stability of the cascaded closed-loop LLOS control system. Noting that the proposed control framework does not make small sideslip angle assumption ($< 5°$) that is used in existing literature [6], [7], [8].
3) We implement the LLOS algorithm successfully for path following control of underactuated ASVs through harbor experiments. The experimental results show that the error of the SUS-LSTM sideslip angle estimator is less than $0.6°$, which is much smaller than that of the traditional estimator, and effectively improves the path following performance.

The structure of this article is outlined as follows. Section II presents the problems statement. Section III describes the proposed SUS-LSTM model structure. Section IV introduces the design of the LLOS guidance law based on the SUS-LSTM estimator and stability analysis. Section V presents hardware experiment on ASVs motion control using the proposed method. Section VI concludes the article.

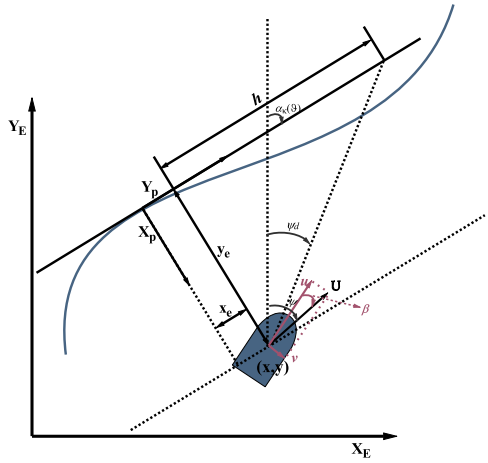

Fig. 1. Geometric diagram illustration of LOS guidance.

II. Problem Statement

The kinematics equations of ASVs can be represented by

$$\begin{cases} \dot{x} = u\cos\psi - v\sin\psi \\ \dot{y} = u\sin\psi - v\cos\psi \\ \dot{\psi} = r \end{cases} \tag{1}$$

where $[x, y, \psi]^T$ is position and orientation of the ASVs relative to the earth-fixed inertial frame, while $[u, v, r]^T$ represents the surge velocities, sway velocities and the angular rate (yaw) in the body-fixed frame, respectively [16].

The geometrical illustration of path following problem is shown in Fig. 1. A preset geometric path $(x_k(\vartheta), y_k(\vartheta))$ is chosen as the reference path, the path-tangential angle is expressed as $\alpha_k(\vartheta) = a\tan2(x_k'(\vartheta), y_k'(\vartheta))$. For an ASV located at (x, y), the path following errors (x_e, y_e) can be delineated as

$$\begin{bmatrix} x_e \\ y_e \end{bmatrix} = \begin{bmatrix} \cos\alpha_k & -\sin\alpha_k \\ \sin\alpha_k & \cos\alpha_k \end{bmatrix}^T \begin{bmatrix} x - x_k(\vartheta) \\ y - y_k(\vartheta) \end{bmatrix}. \tag{2}$$

Differentiating (2), the path following error dynamics of the ASVs can be obtained as

$$\begin{cases} \dot{x}_e = U\cos(\psi - \alpha_k)\cos\beta - U\sin(\psi - \alpha_k)\sin\beta - \dot{\alpha}_k y_e - \mu_p \\ \dot{y}_e = U\sin(\psi - \alpha_k)\cos\beta - U\cos(\psi - \alpha_k)\sin\beta - \dot{\alpha}_k x_e\beta \end{cases} \tag{3}$$

where $U = \sqrt{u^2 + v^2}$ is the resultant speed of the ASVs, $\beta = a\tan2(v, u) > 0$ represents the sideslip angle, and μ_p is the velocity of virtual target along the desired path, which can be expressed as $\mu_p = \dot{\vartheta}\sqrt{x_k'^2(\vartheta) + y_k'^2(\vartheta)}$ [18].

Note that β denotes intersection angle of the ASVs velocity vector U relative to the body-fixed frame, which arises from external environmental forces, such as wind, waves,

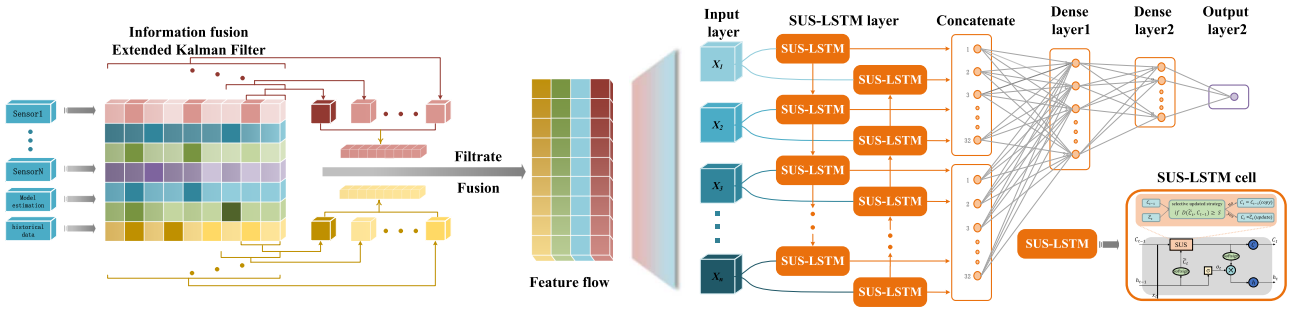

Fig. 2. Overall structure of sideslip angle predictor based on SUS-LSTM.

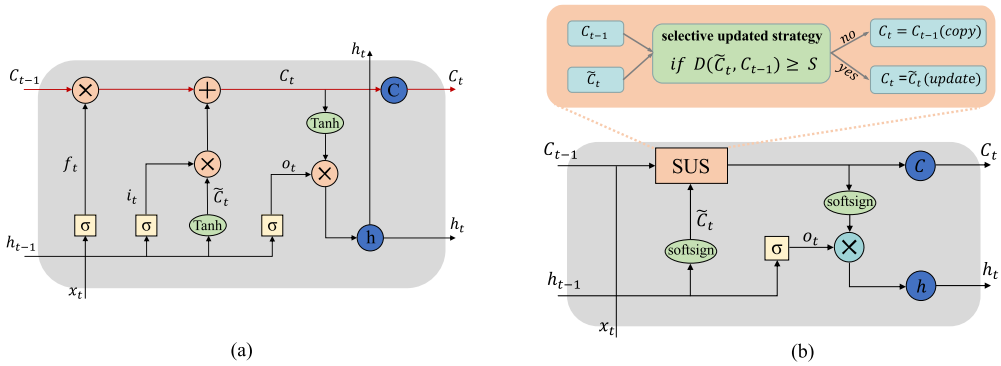

Fig. 3. Cell structure comparison between traditional LSTM and novel SUS-LSTM. (a) Traditional LSTM cell. (b) Novel SUS-LSTM cell.

and currents, or control forces. Let $\xi = \tan\beta$, the (3) can be converted to

$$\begin{cases} \dot{x}_e = u\cos(\psi - \alpha_k) - u\sin(\psi - \alpha_k)\xi + \dot{\alpha}_k y_e - \mu_p \\ \dot{y}_e = u\sin(\psi - \alpha_k) + u\cos(\psi - \alpha_k)\xi - \dot{\alpha}_k x_e. \end{cases} \tag{4}$$

Remark 1: Different from [6], [7], [8], this article extends the range of sideslip angle, and removes the assumption that the β is small (less than 5°) where $\sin(\beta) \approx \beta$ and $\cos(\beta) \approx 1$.

The aim of this article is to design control laws that force ASVs to follow a reference path $\Gamma_k(\vartheta) = (x_k(\vartheta), y_k(\vartheta))$, while contending with an undisclosed time-varying sideslip angle.

III. Sideslip Angle Estimation-Based SUS-LSTM

In this section, to better estimate the unknown and time-varying sideslip angle, we design a RNN called SUS-LSTM, which incorporates a SUS. As shown in Fig. 2, the diagram illustrates the architecture of our proposed lateral sideslip angle estimator, predominantly based on the SUS-LSTM neural network. Next, we will introduce it from the following four aspects.

A. Traditional LSTM Cell

LSTM has the same chain structure as RNN, but the repeating unit has a different structure. The key to LSTM is the cell state. As shown by the red line in Fig. 3(a), the cell state propagates through the conveyor belt-like line located at the top of the cell [13]. It exists throughout the entire LSTM chain system with only a few linear interactions, making it easy for information to propagate and remain constant. However, in the stage of time-series feature extraction with LSTM, there may be issues such as feature redundancy or insufficient feature extraction in the hidden feature information h_t output by the output gate o_t due to the independent feature extraction of the forget gate f_t and input gate i_t [14]. In recent years, theoretical studies, exemplified by [12], have elucidated the geometric traversal of short-term memory within the LSTM model. This characteristic restricts its ability to learn and retain highly fluctuating temporal information in the data.

The above problems may seriously affect LSTM's ability to extract time series features. In order to alleviate the rapid decay rate of LSTM model's long-term memory, enhance the utilization of information in the cell state, learn highly fluctuating temporal information, and reduce the problems of information redundancy or insufficient extraction, we propose an improved LSTM unit structure to solve the above problems.

B. Selective Update Strategy

We improve the traditional LSTM model by using the SUS, which uses $D(\widetilde{C}_t, C_{t-1}) \geq S$ to decide whether to update the cell state or copy the previous hidden state information. The specific structure of the update module SUS is shown in the upper part of Fig. 3(b), and this mechanism can be formalized as follows:

$$C_t = \begin{cases} \widetilde{C}_t, & \text{if } D(\widetilde{C}_t, C_{t-1}) \geq S \\ C_{t-1}, & \text{otherwise} \end{cases} \tag{5}$$

where C_t represents the cell unit state, $D(X, Y) = \sqrt{\sum_{i=1}^{n}(x_i - y_i)^2}$, and S is a predefined parameter. The state at

time step t is updated if the update condition $D(\widetilde{C}_t, C_{t-1}) \geq S$ is satisfied.

The design motivation of SUS is as follows. In SkipRNN [15], a binary update strategy is proposed to reduce the update frequency of hidden states. However, in this model, the update condition of hidden states is independent of the input, and the update frequency increases monotonically. In the RGRU model [20], the method of judging whether a cell should be updated is based on whether the hidden state multiplied by a scalar parameter is greater than the state at the previous time step, thereby reducing the update frequency and enhancing the memory capacity for historical information. In comparison, our proposed method optimizes and clarifies the criteria for selective updating by judging the difference between the hidden state and the previous state to determine whether an update is necessary. Obviously, when there is a significant difference, the hidden state should be updated to effectively capture fluctuating information; otherwise, the hidden state is copied from the previous time step. A clear and simple judgment criterion is more conducive to enhancing the learning ability and long-term memory of extreme data variations, while also facilitating model optimization and execution.

C. Novel SUS-LSTM Cell

In this section, we specifically introduce the construction of the SUS-LSTM cell structure. Considering that the cell state in the LSTM unit has only a few linear interactions in the entire LSTM chain system, information is easier to propagate and remains unchanged. To better utilize the cell state of the LSTM, we use SUS to replace the traditional input and forgetting gates in LSTM, reducing the problem of redundant feature information or insufficient feature extraction caused by the independent extraction of feature information by the forgetting gates and input gates.

We replace the tan$h$ function used in traditional LSTM with a more smooth softsign function [13]. Compared to the tan$h$ function, the softsign function exhibits a smoother gradient, preventing it from becoming excessively small when the input approaches extreme values. This characteristic allows for better mitigation of issues related to gradient vanishing or exploding. Additionally, the softsign function obviates the need for translation and scaling operations, resulting in lower computational overhead. Moreover, the derivative of the softsign function is computationally straightforward. The equation for SUS-LSTM is as follows:

$$\begin{cases} o_t = \text{sigmoid}\left(W_w * [h_{t-1}, x_t, C_{t-1}] + b_o\right) \\ \widetilde{C}_t = \text{softsign}\left(W_c * [h_{t-1}, x_t, C_{t-1}] + b_c\right) \\ C_t = \begin{cases} \widetilde{C}_t, & \text{if } D(\widetilde{C}_t, C_{t-1}) \geq S \\ C_{t-1}, & \text{otherwise} \end{cases} \\ h_t = o_t * \text{softsign}(C_t) \end{cases} \tag{6}$$

where o_t represents the output gate with a sigmoid activation function. $\widetilde{C}_t$ represents the current candidate state with softsign activation function, C_{t-1} represents current candidate state and we have also introduced the cell state as input to it. The unit output, represented by h_t.

We employ softsign as the activation function for the cell candidate state, ensuring that both $\widetilde{C}_t$ and C_{t-1} are vectors within the range of $(-1, 1)$. In update strategy selection, we discern whether to update the cell's hidden state by comparing the Euclidean distance between $\widetilde{C}_t$ and C_{t-1}. Throughout the training process, we predefine the value of S as a vector set at 0.3, with dimensions matching those of the hidden state of the cell unit. We ascertain the optimal value of S by comparing the training outcomes across various S values.

D. Overall Structural Design

As illustrated in the left panel of Fig. 2, we employ an extended kalman filter to filter the obtained information for denoising and multisensor information fusion, so as to enhance the reliability of information. Through correlation analysis, we extract crucial information from the extensive dataset, serving as inputs for the SUS-LSTM neural network. This process significantly enhances data reliability while concurrently mitigating computational burden on shipboard hardware. Detailed elaboration on these procedures will be provided in Section V in this article.

The neural network structure is depicted on the right side of Fig. 2, comprising the input layer, bidirectional SUS-LSTM layer, linear layer, and output layer. In the input layer, each blue cube represents the features entering the network and is arranged temporally. As indicated by the blue arrows in Fig. 2, they are separately fed into the bidirectional SUS-LSTM. The bidirectional SUS-LSTM layer are crucial layers, each SUS-LSTM unit is connected by the orange vertical arrows in the figure, signifying that the output of the previous SUS-LSTM unit serves as the input for the next unit. To effectively utilize outputs from both directions, we connect and fuse the outputs of SUS-LSTM through the orange horizontal arrows in the figure. Following the bidirectional SUS-LSTM layer, two fully connected layers are employed as encoders, linking to the final output layer.

In the SUS-LSTM layers of the neural network, a bidirectional structure is employed. The utilization of this approach in handling time-series data confers superior accuracy and modeling capabilities compared to traditional unidirectional neural networks [11]. This structure enables simultaneous consideration of both past and future data, facilitating a more comprehensive and accurate capturing of temporal features. Consequently, it enhances the overall performance and generalization capability of the model. Meanwhile, the bidirectional structure proves to be more effective in capturing long-term dependency relationships, mitigating issues such as gradient disappearance, thereby further improving the stability of training and prediction [21].

IV. LLOS Guidance Law

A. Guidance Law Design

In this section, based on the proposed SUS-LSTM sideslip angle estimator, an LLOS guidance law was designed to

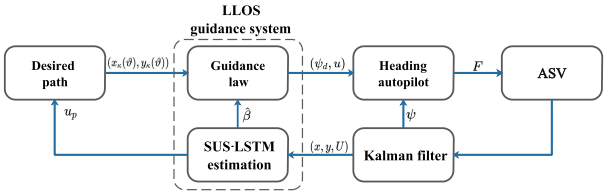

Fig. 4. Path following system combines LLOS guidance with a commercial heading autopilot.

enhance path following performance. The proposed LLOS guidance law is delineated as

$$\psi_d = \alpha_k(\vartheta) + \arctan\left(-\frac{y_e}{\Delta} - \alpha_y\right) \tag{7}$$

where α_y, Δ are virtual control input. The term u_p is designed as

$$u_p = U\cos\left(\psi_d - \alpha_k\right) - U\sin\left(\psi_d - \alpha_k\right)\hat{\xi} + \kappa x_e \tag{8}$$

where κ is control gain, $\hat{\xi}$ is SUS-LSTM estimation. The update speed of the reference path can be described as

$$\dot{\vartheta} = \frac{u\cos\left(\psi_d - \alpha_k\right) - u\sin\left(\psi_d - \alpha_k\right)\hat{\xi} + \kappa\hat{x}_e}{\sqrt{x_k'^2(\vartheta) + y_k'^2(\vartheta)}} \tag{9}$$

because

$$\begin{cases} \sin\left(\arctan\left(-\frac{y_e}{\Delta} - \alpha_y\right)\right) = -\frac{y_e + \Delta\alpha_y}{\sqrt{\Delta^2 + (y_e + \alpha_y)^2}} \\ \cos\left(\arctan\left(-\frac{y_e}{\Delta} - \alpha_y\right)\right) = \frac{\Delta}{\sqrt{\Delta^2 + (y_e + \alpha_y)^2}} \end{cases} \tag{10}$$

and substituting (8) into the equality of (3), set $\alpha_y = \Delta\hat{\xi}$ the error dynamics concerning x_e and y_e can be expressed by

$$\begin{cases} \dot{x}_e = -\kappa x_e + u\sin\left(\psi_d - \alpha_k\right)\tilde{\xi} + \dot{\alpha}_k y_e \\ \dot{y}_e = -c y_e + u\cos\left(\psi_d - \alpha_k\right)\tilde{\xi} - \dot{\alpha}_k x_e \end{cases} \tag{11}$$

where $c = \left(u/\sqrt{\Delta^2 + \left(\hat{y}_e + \Delta\hat{\xi}\right)^2}\right) > 0$, $\tilde{\xi} = \hat{\xi} - \xi$ is error of estimation.

The proposed LLOS guidance law can be effectively employed in conjunction with a commercial heading autopilot system, as illustrated in Fig. 4. A classical proportional integral derivative controller is employed for yaw stabilization in the autopilot system. The control command for steering the vessel is calculated using the following formula:

$$F_{\text{con}} = -K_p\left(\psi - \psi_d\right) - K_i\int_0^t\left(\psi - \psi_d\right)dt - K_d\dot{\psi} \tag{12}$$

where K_p, K_i, K_d are adjustable parameters.

B. Stability Analysis

The LLOS guidance system can be considered as a cascade system consisting of the estimator subsystem and the guidance law subsystem

$$\begin{cases} \mathscr{G}_1 : \begin{cases} \dot{x}_e = -\kappa x_e + u\sin\left(\psi_d - \alpha_k\right)\tilde{\xi} + \dot{\alpha}_k y_e \\ \dot{y}_e = -c y_e + u\cos\left(\psi_d - \alpha_k\right)\tilde{\xi} - \dot{\alpha}_k x_e \end{cases} \\ \mathscr{G}_2 : \tilde{\xi} = \xi - \hat{\xi}. \end{cases} \tag{13}$$

To ensure stability about the proposed closed-loop LLOS guidance system that required the estimation error be within a certain range, indicating that the loss function of the neural network needs to satisfy $\mathcal{L}(\hat{\xi},\xi) = (1/n)\sum(\hat{\xi} - \xi)^2 < \varepsilon$, where $\varepsilon > 0$. During the neural network training process, the loss function $\mathcal{L}(\hat{\xi},\xi)$ becomes a random variable due to the stochastic nature of samples and learning data. In the subsequent discussion, we establish a result to ensure that $\mathcal{L}(\hat{\xi},\xi) < \varepsilon$ holds in probability, drawing inspiration from the work by [22].

Theorem 1: Assuming that the input data for training follows a uniform distribution and training samples are independently sampled from this distribution, for any $\varepsilon > 0$ and $\delta \in (0, 1]$, it can be ensured that there exists a sufficiently large number of training samples N such that

$$P\left\{\mathcal{L}(\hat{\xi},\xi) < \varepsilon\right\} \geq 1 - \frac{R_{\text{emp}}(\hat{\xi},\xi)}{\left(1 - \sqrt{\frac{c-1}{N\delta}}\right)\varepsilon} \tag{14}$$

where c is a constant satisfying $c \geq 1$, $R_{\text{emp}}(\hat{\xi},\xi)$ represents a bounded empirical error with a small value, which can be expressed as $R_{\text{emp}}(\hat{\xi}_k,\xi_k) = (1/N)\sum_{k=1}^{N}\mathcal{L}(\hat{\xi},\xi)$.

Proof: Taking into account the non-negativity of $\mathcal{L}(\hat{\xi},\xi)$ and for $\varepsilon > 0$ utilizing Markov's inequality, we acquire

$$P\left\{\mathcal{L}(\hat{\xi},\xi) \geq \varepsilon\right\} \leq \frac{E[\mathcal{L}(\hat{\xi},\xi)]}{\varepsilon} \tag{15}$$

where $E[\mathcal{L}(\hat{\xi},\xi)]$ as defined in [23] denotes the generalization error, and it is expressed as

$$E[\mathcal{L}(\hat{\xi},\xi)] = R_{\text{gen}}(\hat{\xi},\xi) = \int(\hat{\xi},\xi)dF(\xi \mid \boldsymbol{x}) \tag{16}$$

utilizing the inequality (15), we can constrain the probability of $\mathcal{L}(\hat{\xi},\xi) < \varepsilon$ as

$$P\left\{\mathcal{L}(\hat{\xi},\xi) < \varepsilon\right\} \geq 1 - \frac{R_{\text{gen}}(\hat{\xi},\xi)}{\varepsilon}. \tag{17}$$

Due to the positivity of the variance $V[\mathcal{L}(\hat{\xi},\xi)]$ of the loss function $\mathcal{L}(\hat{\xi},\xi)$ and it satisfies $V[\mathcal{L}(\hat{\xi},\xi)] = E[\mathcal{L}^2(\hat{\xi},\xi)] - [E[\mathcal{L}(\hat{\xi},\xi)]]^2$, there exists $c \geq 1$ such that

$$V[\mathcal{L}(\hat{\xi},\xi)] \leq (c-1)E^2\left[\mathcal{L}\left(\boldsymbol{U}_{\boldsymbol{\theta}},\boldsymbol{U}^*\right)\right] \leq (c-1)R_{\text{gen}}^2(\hat{\xi},\xi) \tag{18}$$

because the training sample data $x(k)$ are independent of each other, the upper bound about the $V[R_{\text{emp}}(\hat{\xi},\xi)]$ can be computed using the inequality in (18)

$$V[R_{\text{emp}}(\hat{\xi},\xi)] = \frac{1}{M}V[\mathcal{L}(\hat{\xi},\xi)] \leq \frac{c-1}{M}R_{\text{gen}}^2(\hat{\xi},\xi). \tag{19}$$

The expectation of $R_{\text{emp}}(\hat{\xi},\xi)$ can be calculated as

$$E[R_{\text{emp}}(\hat{\xi},\xi)] = \frac{1}{M}\sum_{k=1}^{M}R_{\text{gen}}(\hat{\xi},\xi) = R_{\text{gen}}(\hat{\xi},\xi) \tag{20}$$

by utilizing the inequality (19) and (20), using Chebyshev's inequality, setting $\sigma = \sqrt{(c - 1/N\delta)}R_{\text{gen}}(\hat{\xi},\xi)$ we can get

$$P\left\{\mid R_{\text{emp}}(\hat{\xi},\xi) - R_{\text{gen}}(\hat{\xi},\xi) \mid < \sqrt{\frac{c-1}{N\delta}}R_{\text{gen}}(\hat{\xi},\xi)\right\} \geq 1 - \delta. \tag{21}$$

The empirical error is demonstrated to be smaller than the generalization error in [24], we can conclude that the upper bound of $R_{\text{gen}}(\hat{\xi},\xi)$ adheres to the following constraint:

$$P\left\{R_{\text{gen}}\left(\hat{\xi},\xi\right)\leq\left(1-\sqrt{\frac{c-1}{N\delta}}\right)^{-1}R_{\text{emp}}(\hat{\xi},\xi)\right\}\geq 1-\delta. \tag{22}$$

Substituting (22) in equation (15), we obtain the inequality presented in (14), thereby concluding the proof. Therefore, the estimation error $\tilde{\xi}$ of the sideslip angle estimation subsystem $\mathscr{G}_2$ based on SUS-LSTM is bounded, and the bounded probability approaches to 1 as the number of samples N increases. □

Next, the stability of closed-loop cascade system is analyzed.

Theorem 2: The subsystem $\mathscr{G}_1$ is conceived as a system with states x_e, y_e and bounded input $\tilde{\xi}$. Under the conditions of $\{(\kappa-u/(2\varepsilon_1)),(c-u/(2\varepsilon_2))\}>0$, this system demonstrates input-to-state stability, with $\varepsilon_1,\varepsilon_2$ and κ denoting prescribed positive constants.

Proof: Consider the candidate Lyapunov function

$$V=\frac{1}{2}x_e^2+\frac{1}{2}y_e^2 \tag{23}$$

taking the derivative of the above equation yields

$$\dot{V}=-\kappa x_e^2-cy_e^2+u\sin\left(\psi_d-\alpha_k\right)x_e\tilde{\xi}+u\cos\left(\psi_d-\alpha_k\right)y_e\tilde{\xi} \tag{24}$$

by Young's inequality

$$\begin{cases}u\sin\left(\psi_d-\alpha_k\right)x_e\tilde{\xi}\leq\frac{u}{2\varepsilon_1}\left|x_e\right|^2+\frac{u\varepsilon_1}{2}|\tilde{\xi}|^2\\ u\cos\left(\psi_d-\alpha_k\right)y_e\tilde{\xi}\leq\frac{u}{2\varepsilon_2}\left|y_e\right|^2+\frac{u\varepsilon_2}{2}|\tilde{\xi}|^2\end{cases} \tag{25}$$

consequently

$$\begin{aligned}\dot{V}&\leq-\left(\kappa-\frac{u}{2\varepsilon_1}\right)x_e^2-\left(c-\frac{u}{2\varepsilon_2}\right)y_e^2+\frac{u}{2}\left(\varepsilon_1+\varepsilon_2\right)|\tilde{\xi}|^2\\&\leq-2h_{\min}\|E\|^2+\frac{u}{2}\left(\varepsilon_1+\varepsilon_2\right)|\tilde{\xi}|^2\end{aligned} \tag{26}$$

where $h_{\min}=\min\left\{\left(\kappa-u/\left(2\varepsilon_1\right)\right),\left(c-u/\left(2\varepsilon_2\right)\right)\right\}>0$, $E=[y_e,x_e]$, since

$$\|E\|\geq\frac{\sqrt{u\varepsilon_1}|\tilde{\xi}|}{\sqrt{h_{\min}}}+\frac{\sqrt{u\varepsilon_2}|\tilde{\xi}|}{\sqrt{h_{\min}}}\geq\sqrt{\frac{u\left(\varepsilon_1+\varepsilon_2\right)|\tilde{\xi}|^2}{h_{\min}}} \tag{27}$$

it yields that

$$\begin{aligned}\dot{V}&\leq-\frac{h_{\min}\|E\|^2}{2}-\left(\frac{h_{\min}\|E\|^2}{2}-\frac{u}{2}\left(\varepsilon_1+\varepsilon_2\right)|\tilde{\xi}|^2\right)\\&\leq-h_{\min}\|E\|^2/2.\end{aligned} \tag{28}$$

Choosing $\alpha_1(\|E\|)=\alpha_2(\|E\|)=\|E\|^2/2=V$, then there exists a class $\mathcal{K}$ function $\rho(x)=\sqrt{u\left(\varepsilon_1+\varepsilon_2\right)/2}x$ such that $\gamma=\alpha_1^{-1}\cdot\alpha_2\cdot\rho=\rho$ and a class $\mathcal{KL}$ function $\delta_{\mathcal{KL}}\left(E\left(t_0\right),t\right)=e^{-(h_{\min}/2)t}E\left(t_0\right)$, and

$$\|E(t)\|\leq\delta_{\mathcal{KL}}\left(E\left(t_0\right),t\right)+\rho(|\tilde{\xi}|) \tag{29}$$

from Theorem 1 it follows that $P\{\mathcal{L}(\hat{\xi},\xi)<\varepsilon\}\to 1$. That is, the value of $\tilde{\xi}$ in subsystem $\mathscr{G}_2$ is in very small range. Therefore the subsystem $\mathscr{G}_1$ is input-to-state stability according to Theorem 2.1 and Definition 4.7 in [17]. □

Fig. 5. ASV for experimental and satellite map of experimental environment.

TABLE I
PEARSON CORRELATION COEFFICIENTS BETWEEN EACH SIGNAL AND THE SIDESLIP ANGLE

Signal	X	Y	Pitch	Roll	Yaw	ϕ_d	X_d	Y_d
Value	−0.182	0.31	−0.22	0.26	0.33	−0.23	−0.22	0.29

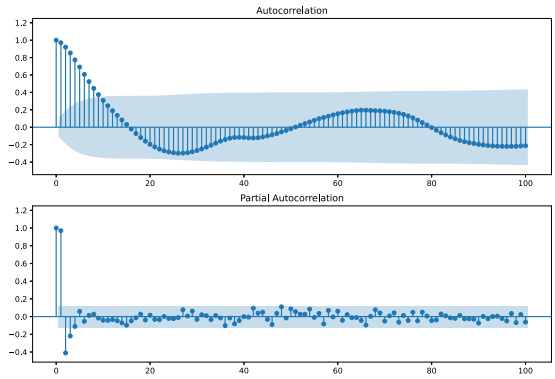

Fig. 6. Autocorrelation and partial autocorrelation analyses plots of the sideslip angle signal.

V. IMPLEMENTATION TO ASVS

We apply the proposed SUS-LSTM-based LLOS guidance law to ASVs platform and conduct harbor experiments. As depicted in Fig. 5, the entire mass of the ASVs is 5.4 kg, with a length of 1.1 m, axis distance 0.36 m and its maximum power output 36 w [17].

A. Learning SUS-LSTM

The underactuated ASVs are equipped with a diverse array of sensors, including the MicroL3GD20H and MicroLSM303D from STMicroelectronics, the MPU6000 from Invensense, and the GPS M8 from u-blox, to capture various motion information of the ASVs. However, the presence of random noise in the acquired information due to sensor errors and external disturbances, as well as exist the issue of information overload. To address this, as illustrated on the left side of Fig. 2, we employ an extended Kalman filter to filter the obtained information for denoising and multisensor information fusion, so as to enhance the reliability of information. Considering the processing capabilities of the ASVs onboard processor, and to improve computational efficiency and reduce the computational burden, further information selection is performed. We calculate

TABLE II
PERFORMANCE FOR ALL METHODS

Method	Straight Path			Circular Path			S-Shaped Path		
	RMSE	MAE	SMAPE	RMSE	MAE	SMAPE	RMSE	MAE	SMAPE
GRU [10]	0.189	0.132	10.755%	0.486	0.288	20.37%	0.832	0.503	31.13%
LSTM [19]	0.185	0.120	10.516%	0.441	0.313	21.19%	0.792	0.491	28.14%
Bi-LSTM [11]	0.176	**0.119**	**9.406%**	0.392	0.296	20.45%	0.712	0.451	27.64%
LSTM-EFG [13]	0.179	0.126	9.927%	0.347	0.209	19.51%	0.762	0.472	27.14%
SkipGRU [15]	0.182	0.128	10.142%	0.235	0.173	17.92%	0.662	0.411	24.13%
SUS-LSTM (ours)	**0.173**	0.121	9.637%	**0.192**	**0.131**	**13.44%**	**0.413**	**0.332**	**19.15%**

Note: Bold values indicate the best results.

Pearson correlation coefficients between the available information, such as velocity, position, control signals, and the sideslip angle signal, to select the optimal feature inputs for the SUS-LSTM.

As illustrated in Table I, we have chosen the eight most highly correlated features as inputs for the neural network. Simultaneously, we conducted autocorrelation function (ACF) and partial autocorrelation function (PACF) analyses on the sideslip angle signal, with a sampling interval of 1 s. The Fig. 6(a) shows the ACF of the sideslip angle, indicating that the time series does not exhibit truncation or tailing phenomena, suggesting a strong autocorrelation in the sideslip angle sequence. The lower part of Fig. 6 displays the PACF of the sideslip angle. It is evident from the graph that the sideslip angle signal exhibits correlation within a 4-s time series. Therefore, we chose a time sequence of 4 s, with a control sampling frequency of 5 Hz in ASVs, resulting in a sequence step size of 20.

The deep learning models employed in this article were developed using the Python programming language and implemented on the PyTorch framework. All experiments were performed on a Linux server in the same environment. We evaluated the performance of SUS-LSTM through comprehensive comparisons with several baseline methods, including GRU [10], LSTM [19], Bi-LSTM [11], LSTM-EFG [13], and SkipGRU [15], via experimental trials. Regarding model evaluation, the selected assessment metrics for all predictive models in this article encompass mean absolute error (MAE), root mean square error (RMSE), and symmetric mean absolute percentage error (SMAPE), which are commonly used in almost all time-series prediction [11], [13], [15], [19].

Table II summarizes the results of predictive performance for all models across three different tracking trajectories. From the Table II, it is evident that the proposed SUS-LSTM model exhibits significant advantages over other models in all tracking scenarios. For instance, in contrast to the state-of-the-art algorithm, the SUS-LSTM model exhibits a 21.27% increase in RMSE accuracy in circular path tracking tasks. Simultaneously, when faced with datasets characterized by intricate oscillations, such as the S-shaped path following task, the model's performance improve 19.24%.

B. Hardware Implementation

To evaluate the effectiveness and superiority of the LLOS, we designed hardware experiments employing two distinct reference paths: (a) straight-line path following; and (b) S-shaped path following.

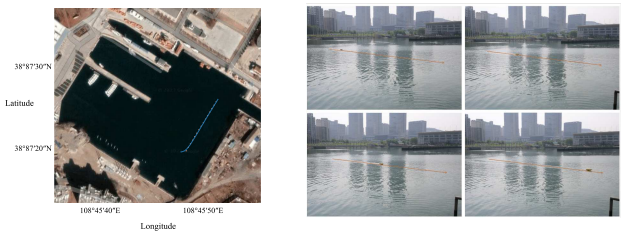

(a) (b)

Fig. 7. Case A: Path following trajectory of ASV and real shots. (a) Path following trajectory. (b) Real shots.

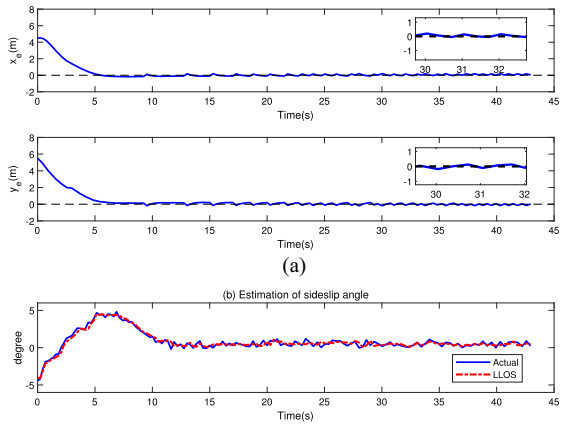

(a)

(b)

Fig. 8. Case A: Path following errors of ASV and estimation of sideslip angle. (a) Along-tracking and cross-tracking errors. (b) Estimation of sideslip angle.

1) Case A: Straight Line Path Following of ASVs: In this case study, chosen control parameters are specified as follows: $\Delta = 4$, $\kappa = 7$, with a baseline ship velocity of 1.5 m/s. Fig. 7(a) shows the trajectory of the ASVs on the satellite map, and Fig. 7(b) displays the practical implementation of our proposed method during the experiment. It can be observed from Fig. 8(a) that the path following errors converge to zero. Fig. 8(b) illustrates the depiction of the estimated sideslip angles by our proposed SUS-LSTM sideslip angle predictor, with the estimation error is less than 0.32°.

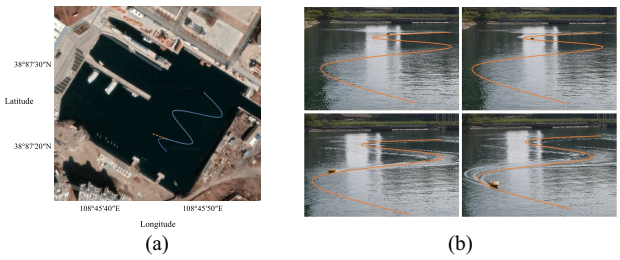

(a) (b)

Fig. 9. Case B: Path following trajectory of ASV and real shots. (a) Path following trajectory. (b) Real shots.

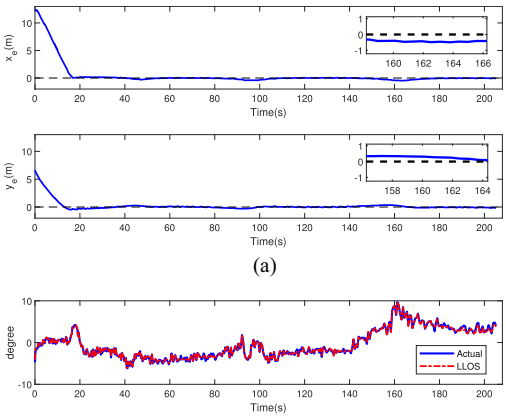

(a) (b)

Fig. 10. Case B: Path following errors of ASV and estimation of sideslip angle. (a) Path following trajectory. (b) Real shots.

2) Case B: S-Shaped Path Following of ASVs: In practical applications, ASVs are frequently used to accomplish various complex tasks, and the path following of ASVs under time-varying yaw angles is also complex. In order to better fit real-world scenarios and verify the effectiveness of our proposed algorithm, in this section, we consider the complex S-shaped path of ASVs under time-varying sideslip angle. For this specific case, the selected control parameters are as follows: $\Delta = 3, \kappa = 6$ with a baseline ship velocity of 1.3 m/s. Fig. 9(a) shows the trajectory of the ASVs on the satellite map in Case B, and Fig. 9(b) displays the real shots for practical implementation of the proposed method. Fig. 10(a) shown that the tracking error can be stabilized quickly even under the influence of large steering changes and perturbations. Fig. 10(b) illustrates the depiction of the estimated sideslip angles by our proposed SUS-LSTM sideslip angle predictor. The estimation error is less than 0.52°.

3) Case C: Circle Path Following of ASVs: In addition, we have included circular path following tasks to compare with the ALOS algorithm [6], aiming to demonstrate the superiority of the proposed method. The ALOS guidance law is as follows:

$$\begin{cases} \psi_{\text{ALOS}} = \gamma_p + \text{atan}\left(-\frac{1}{\Delta} - \hat{\beta}\right) \\ \dot{\hat{\beta}} = l\frac{U\Delta}{\sqrt{\Delta^2+\left(y_e+\Delta\hat{\beta}\right)^2}}, l > 0 \end{cases} \tag{30}$$

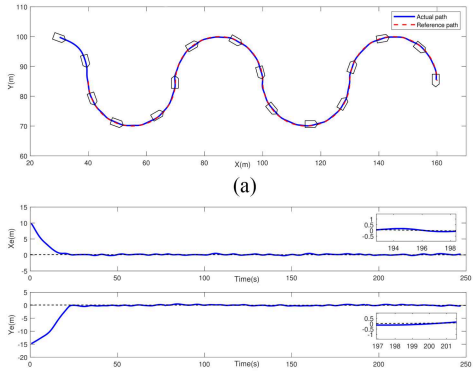

(a) (b)

Fig. 11. Case C: Trajectory of ASV and path following errors. (a) Path following trajectory. (b) Along-tracking and cross-tracking errors.

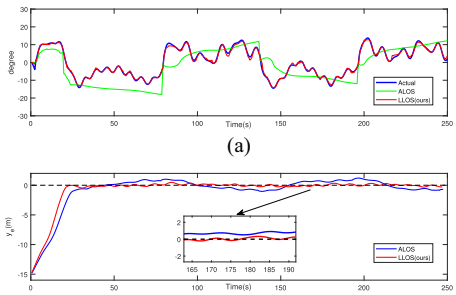

(a) (b)

Fig. 12. Case C: Comparison of estimated sideslip angle and cross-tracking error. (a) Comparison of estimated sideslip angle. (b) Cross-tracking error.

In the comparative simulation of this section, the selected path consists of interconnected circular segments, each with a radius of 15 m. We compare our proposed LLOS guidance method with ALOS, selecting an adaptive $l = 2 \times 10^{-3}$.

Fig. 11(a) demonstrates that the proposed LLOS guidance algorithm enables the ASV to accurately follow the reference path. Fig. 11(b) indicates that the track error converge to zero within a very tight range. In Fig. 12(a), it is illustrated that ALOS exhibits some capability in estimating large time-varying sideslip angles, although its performance is suboptimal. In contrast, our proposed sideslip angle predictor based on SUS-LSTM demonstrates superior estimation of sideslip angles, with an estimation error bounded to less than 0.43°. As shown in Fig. 12(b), compared to ALOS, the proposed LLOS guidance algorithm significantly enhances path following performance and transient response under conditions of substantial time-varying sideslip angles.

VI. Conclusion

A novel sideslip angle estimator named SUS-LSTM is proposed to address the issue of poor performance of traditional estimate compensation methods when facing with big amplitude and fluctuating sideslip angle scenarios, leading to the path following performance deteriorates of underactuated ASVs in

LOS guidance. The SUS-LSTM integrates a selective updating strategy to more directly preserve cell state information, enhancing long-term memory and learning capabilities for extreme information, thus fulfilling the demand for estimate fluctuating sideslip angles. Based on the proposed SUS-LSTM, the LLOS is designed. Furthermore, under mild conditions, we theoretically prove the input-to-state stability about the closed-loop cascaded control system LLOS combined with the heading controller. Simulation and hardware experiments have confirmed the effectiveness and superiority of the proposed algorithm.

REFERENCES

[1] H. Liang, H. Li, J. Gao, R. Cui, and D. Xu, "Economic MPC-based planning for marine vehicles: Tuning safety and energy efficiency," *IEEE Trans. Ind. Electron.*, vol. 70, no. 10, pp. 10546–10556, Oct. 2023.

[2] S. Wang, M. Sun, Y. Xu, J. Liu, and C. Sun, "Predictor-based fixed-time LOS path following control of underactuated USV with unknown disturbances," *IEEE Trans. Intell. Veh.*, vol. 8, no. 4, pp. 2088–2096, Mar. 2023.

[3] N. Gu, D. Wang, Z. Peng, J. Wang, and Q. Han, "Advances in line-of-sight guidance for path following of autonomous marine vehicles: An overview," *IEEE Trans. Syst. Man, Cybern. A*, vol. 53, no. 1, pp. 12–28, Jan. 2023.

[4] T. Fossen and K. Pettersen, "On uniform semiglobal exponential stability (USGES) of proportional line-of-sight guidance laws, " *Automatica*, vol. 50, pp. 2912–2917, Nov. 2014.

[5] A. Lekkas and T. Fossen, "Integral LOS path following for curved paths based on a monotone cubic Hermite spline parametrization," *IEEE Trans. Control Syst. Technol.*, vol. 22, no. 6, pp. 2287–2301, Nov. 2014.

[6] T. Fossen, K. Pettersen, and R. Galeazzi, "Line-of-sight path following for Dubins paths with adaptive sideslip compensation of drift forces," *IEEE Trans. Control Syst. Technol.*, vol. 23, no. 2, pp. 820–827, Mar. 2015.

[7] L. Liu, D. Wang, Z. Peng, and H. Wang, "Predictor-based LOS guidance law for path following of underactuated marine surface vehicles with sideslip compensation," *Ocean Eng.*, vol. 124, no. 15, pp. 340–348, Sep. 2016.

[8] L. Liu, D. Wang,and Z. Peng, "ESO-based line-of-sight guidance law for path following of underactuated marine surface vehicles with exact sideslip compensation," *IEEE J. Ocean. Eng.*, vol. 42, no. 2, pp. 477–487, Apr. 2017.

[9] L. Hao, Z. Yang, and Y. Liu. "TRCA-Net: Stronger U structured network for human image segmentation," *Neural Comput. Appl.*, vol. 35, no. 3, pp. 9627–9635, May 2023.

[10] T. Gröber, S. Lupberger, M. Unterreiner, and D. Schramm, "A hybrid approach to side-slip angle estimation with recurrent neural networks and kinematic vehicle models," *IEEE Trans. Intell. Veh.*, vol. 4, no. 1, pp. 39–47, Mar. 2019.

[11] C. Chen, N. Lu, B. Jiang, Y. Xing, and Z. Zhu, "Prediction interval estimation of aeroengine remaining useful life based on bidirectional long short-term memory network," *IEEE Trans. Instrum. Meas.*, vol. 70, no. 1, pp. 1–13, Nov. 2021

[12] J. Zhao et al., "Do RNN and LSTM have long memory," in *Proc. 36th Int. Conf. Mach. Learn.*, vol. 119, 2020, pp. 11365–11375.

[13] R. Yu et al., "LSTM-EFG for wind power forecasting based on sequential correlation features," *Future Gener. Comput. Syst.*, vol. 93, no. 5, pp. 33–42, Apr. 2019.

[14] B. Zhang et al., "A novel encoder-decoder model based on read-first LSTM for air pollutant prediction," *Sci. Total Environ.*, vol. 765, no. 15, pp. 1–15, Apr. 2021.

[15] V. Campos, B. Jou, X. Giró-i-Nieto, J. Torres, and S. Chang, "Skip RNN: Learning to skip state updates in recurrent neural networks," in *Proc. 6th Int. Conf. Learn. Represent. (ICLR)*, 2018, pp. 1–17.

[16] L. Hao, H. Zhang, T. Li, B. Lin, and C. Chen, "Fault tolerant control for dynamic positioning of unmanned marine vehicles based on T-S fuzzy model with unknown membership functions," *IEEE Trans. Veh. Technol.*, vol. 70, no. 1, pp. 146–157, Jan. 2021.

[17] L. Hao, R. Wang, C. Shen, and Y. Shi, "Trajectory tracking control of autonomous underwater vehicles using improved tube-based model predictive control approach," *IEEE Trans Ind. Inform.*, vol. 20, no. 4, pp. 5647–5657, Apr. 2024.

[18] W. Zheng and G. Chen, "An accurate GRU-based power time-series prediction approach with selective state updating and stochastic optimization," *IEEE Trans. Cybern.*, vol. 52, no. 12, pp. 13902–13914, Dec. 2022.

[19] R. Jin, Z. Chen, K. Wu, M. Wu, X. Li, and R. Yan, "Bi-LSTM-based two-stream network for machine remaining useful life prediction," *IEEE Trans. Instrum. Meas.*, vol. 71, no. 1, pp. 1–10, Apr. 2022.

[20] R. Wang, H. Li, B. Liang, Y. Shi, and D. Xu, "Policy learning for nonlinear model predictive control with application to USVs," *IEEE Trans. Ind. Electron.*, vol. 71, no. 4, pp. 4089–4097, Apr. 2024.

[21] Z. Tu, F. He, and D. Tao, "Understanding generalization in recurrent neural networks," in *Proc. Int. Conf. Learn. Representations*, 2020, pp. 1–17.

[22] R. M. Kil and I. Koo, "Generalization bounds for the regression of real-valued functions," in *Proc. 9th Int. Conf. Neural Inf. Process.*, 2002, pp. 1766–1770.

[23] M. Krstić, I. Kanellakopoulos, and P. Kokotovic, *Nonlinear and Adaptive Control Design*. New York, NY, USA: Wiley, ch. 5, pp. 185–232, 1995.

[24] S. Hochreiter and J. Schmidhuber, "Long short-term memory," *Neural Comput.*, vol. 9, no. 8, pp. 1735–1780, Nov. 1997

Li-Ying Hao (Senior Member, IEEE) was born in Jilin, China. She received the M.S. and Ph.D. degrees in control science and engineering from the Northeastern University, Shenyang, China, in 2008 and 2013, respectively.

From 2013 to 2016, she was with the College of Information Engineering, Dalian Ocean University, Dalian, China. From 2015, she was a Visiting Scholar with the Department of Electrical Engineering, Yeungnam University, Kyongsan, South Korea. In 2017, she joined with Dalian Maritime University, Dalian, China, and she is currently a Professor with the Department of Automation, Dalian Maritime University. From 2019 to 2020, she was a Visiting Scholar with the Department of Mechanical Engineering, University of Victoria, British Columbia, Canada. Her research interests include robust fault-tolerant control, model predictive control, sliding mode control, and deep learning with an emphasis on applications in marine vehicles.

Dr. Hao was an Honoree of Outstanding Young Talents in Dalian, China, in 2022.

Yun-Peng Liu received the B.S. degree in electronic information engineering from the Intelligent Manufacturing College, Huanghuai University, Zhumadian, China, in 2020. He is currently toward the M.S. degree in control engineering with Dalian Maritime University, Dalian, China.

His research interests include machine learning, guidance and control.

Zhi-Jie Wu received the M.S. degree in electronic information in 2023, from Dalian Maritime University, Dalian, China, where she is currently working toward the Ph.D. degree in control science and engineering.

Her research interests include model predictive control and fault-tolerant control.

Chao Shen (Member, IEEE) received his B.E. degree in automation engineering and M.Sc. degree in control science and engineering from the Northwestern Polytechnical University, Xi'an, China in 2009 and 2012, respectively, and the Ph.D. degree in mechanical engineering from the University of Victoria, Victoria, Canada, in 2018.

He is currently an Assistant Professor with the Department of Systems and Computer Engineering, Carleton University, Ottawa, Canada. Before joining with Carleton University, he was a Postdoctoral Researcher with the Real-time Adaptive Control Engineering Lab, University of Michigan, Ann Arbor, USA. His research interests include control theory, machine learning, and optimization, and their applications in robotics systems, mechatronics systems, and industrial processes.

Dr. Shen was the winner of the 2018 IEEE SMCS Thesis Grant Initiative for his Ph.D. thesis on model predictive control for underwater robotics; the recipient of the Natural Science and Engineering Research Council of Canada (NSERC) Postdoctoral Fellowship in 2020. He served as an Associate Guest Editor for Special Issues in *IET Control Theory and Applications, Frontiers in Control Engineering* and in *Journal of Marine Science and Engineering*.